Signature of plasmon excitations in the stopping ratio of fast hydrogen clusters

S. M. Shubeita, M. A. Sortica, P. L. Grande, and J. F. Dias
Instituto de Física da Universidade Federal do Rio Grande do Sul, Avenida Bento Gonçalves 9500, 91501-970 Porto Alegre, Rio Grande do Sul, Brazil

N. R. Arista
División Colisiones Atômicas, Centro Atômico Bariloche, Instituto Balseiro, RA-8400 San Carlos de Bariloche, Rio Negro, Argentina
(Received 1 October 2007; revised manuscript received 18 December 2007; published 17 March 2008)

In the present work, we have explored the interference effects which arise when H_2^+ and H_3^+ cluster ions interact with a thin layer of SiO_2 in order to obtain a clear signature of plasmon excitations induced by these energetic projectiles. For this purpose, high-energy-resolution experiments were carried out as a function of the incoming projectile energy, covering an energy range between 40 and 200 keV/amu. The ratio R_n between the energy loss of the cluster and the sum of the energy loss of its constituents has a steep increase between 70 and 100 keV/amu for both cluster ions, which is associated with the plasmon excitation threshold.

DOI: 10.1103/PhysRevB.77.115327 PACS number(s): 79.20.Ap, 34.50.Bw, 34.10.+x, 36.40.−c

I. INTRODUCTION

Plasmon excitation (collective oscillations of valence electrons) is a well established mechanism of particle (ion or electrons) energy loss and plays a central role in different areas of science (from electrochemistry to plasmonics).[1] One of the main differences between electronic and ionic plasmon excitations is that the ions are able to excite plasmons at buried layers or nanoparticles deep under the surface. In the case of thin films, different electron-based techniques have been used to study plasmon excitations.[2–4] One example is the electron energy-loss spectroscopy technique,[5] where the energy of the transmitted electrons is recorded. This technique, however, proved not to be well suited for experiments using energetic ions since the energy-loss spectrum of the transmitted ions stems from multiple scattering events, which mask the effect due to the plasmon excitations.[6] Even for the stopping power measurements, no structures have ever been observed at the plasmon threshold energy.[7] Therefore, in order to evaluate the plasmon excitation induced by ions, an indirect method has been employed. In this method, the energy distribution of excited electrons resulting from the ion impact is measured, and usually, through the derivatives of the energy spectrum, the plasmon excitation contribution is evaluated.[6,8–10]

While most of these experiments made use of protons impinging on metals, very few have been carried out using ionic molecules,[11] although early experiments showed the potentialities of channeling experiments with molecules for the observation of plasmon excitation.[12] In this work, we take advantage of the vicinage effect[11,13] observed in the interaction of ionic hydrogen clusters with thin films to enhance the changes in the energy spectrum that take place at the energy threshold for plasmon excitation, since the cross section for plasmon production is very sensitive to the interference arising from the moving fragments.

The interaction of cluster ions with matter is more complex when compared to the case of single ions. Indeed, the Coulomb explosion[12] and vicinage effects[11,13] play a central role and are connected with the excitation pattern of the target electrons generated by the simultaneous interaction of fragment ions moving in a correlated way within the solid. The molecules dissociate after passing the first monolayers [the breakup cross section is about $(5-10)\times 10^{-16}$ cm^2 (Ref. 14 and 15)] and get stripped of all their electrons for energies larger than 100 keV/amu.[16] The moving ionic fragments repel each other via mutual quasi-Coulomb forces and excite the electronic medium coherently (vicinage effect). The Coulomb explosion leads to a broadening of the energy-loss distribution of the ionic fragments, but causes only a minor effect on their mean energy loss or stopping power as long as the separation of the fragments remains constant. On the other hand, the vicinage effect may increase or decrease the energy loss of the fragments depending on the internuclear distances of the fragments. Thus, the stopping ratio R between the energy loss of the cluster and the sum of the energy loss of its constituents will largely depend on the vicinage effect and only indirectly on the Coulomb explosion itself.

Apart from some measurements involving channeling of cluster ions,[17–21] the usual approach to study the Coulomb explosion and vicinage effects relies on the use of swift hydrogen molecules interacting with amorphous targets. In the seminal work of Brandt *et al.*,[13] thin carbon and gold foils were bombarded with H_2^+ and H_3^+ ions in order to measure the stopping ratio R_n, which corresponds to the energy loss of the H_n^+ cluster divided by the sum of the energy losses of the independent protons. A clear situation of the data from these and other experimental work is shown in the comprehensive compilation carried out in Ref. 11. In particular, the experimental results involving the interaction of hydrogen clusters with carbon foils show large fluctuations of the R_n data as a function of the projectile energy. Moreover, a comparison of the data coming from independent laboratories indicates a lack of compatibility among the results. These effects could be the result of the transmission technique employed in such experiments, which is sensitive to both carbon foil thickness (due to the effects of the Coulomb explosion on the ratio R_n) and to problems related with the degradation of the foils during the experiments. In this scenario, it was practically impossible to draw any definite conclusions about the role

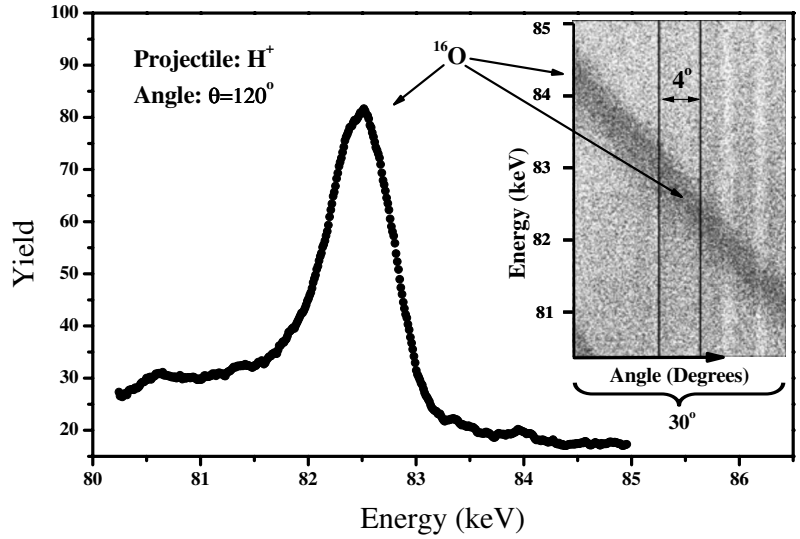

FIG. 1. A typical 1D energy spectrum obtained for backscattered protons in SiO_2 film through the MEIS technique. In this experiment, the proton energy was 100 keV. The inset shows a 2D spectrum with the angular window (4°) from which the 1-D spectrum shown in the figure was derived. The total angular acceptance of the system is 30°. See text for further explanation.

played by fundamental processes like the plasmon excitation through Coulomb interactions.

Since the experimental scenario described above hampered any attempt to observe the structure associated with the plasmon excitation threshold, we carried out measurements of the energy loss of swift H_2^+ and H_3^+ cluster ions when interacting with very thin SiO_2 films using the medium energy ion scattering (MEIS) technique.[22] The high energy resolution of the MEIS technique, associated with the high quality (small roughness) of the thin SiO_2 films employed in the experiments, have allowed a direct observation of the energy threshold for plasmon excitations induced by these ions.

II. EXPERIMENTAL PROCEDURE

For the targets, we have used commercially available SIMOX-type (where SIMOX denotes separation by implanted oxygen) structures, from which only the crystalline Si ⟨100⟩ was used for the oxidation procedure. The samples were cleaned and etched according to a specific protocol, which included the use of de-ionized H_2O, H_2O_2, NH_4OH, and HF (40%). In this way, we were able to remove the native surface oxide layer of the SIMOX sample. Right after the cleaning and/or etching procedure, the samples were kept in clean air in order to develop a thin oxide layer on top of the exposed Si ⟨100⟩ crystal. This naturally grown SiO_2 layer builds up as a function of time and its thickness was evaluated during the experiments. In all cases, the samples prepared in such a way had a thickness ranging from 10 to 25 Å. These films are thin enough to prevent undesirable effects arising from the Coulomb explosion.

The experiments were carried out at the Ion Implantation Laboratory of the Physics Institute (Federal University of Rio Grande do Sul). Beams of H^+, H_2^+, and H_3^+ were delivered by a 500 kV electrostatic accelerator. For the H_2^+ cluster, 11 different energies ranging from 40 to 200 keV/amu were studied, while for H_3^+ clusters, a total of 8 energies (from 40 to 150 keV/amu) were analyzed. The beam energy spreading of the machine is about 80 eV for protons at 150 keV.[23] The MEIS chamber, which accommodates a three-axis goniometer and the detection system, was kept under a pressure of the order of 10^{-7} mbar. Prior to each experiment, the beam was aligned with the Si ⟨100⟩ axis in order to decrease the yield of backscattered protons in silicon, thus enhancing the signal-to-noise ratio of the oxygen peak in the backscattering spectrum.

Figure 1 presents a typical energy spectrum obtained from the MEIS experiment under channeling conditions. Indeed, thanks to the channeling procedure, the ratio between the oxygen peak and the background is pretty good, namely, about 3.5. A detailed description of the detection system and the accompanying electronics setup can be found elsewhere.[22,24,25] In a typical MEIS experiment, a fraction of the protons backscattered in the target enter in the toroidal electrostatic analyzer, whose angular acceptance is 30°, and are analyzed in angle and energy leading to two-dimensional (2D) spectra as shown in the inset of Fig. 1. In this figure, lighter (darker) dots are associated with low (high) count rates for events corresponding to particular ion energy and scattering angle. The 2D spectrum has to be projected onto the energy axis at certain angular bins in order to allow the adequate processing of the information contained in them. Although it is possible to obtain one energy spectra per angle bin (in this case, 0.08°), the best way is to aggregate several angle bins in just one, improving significantly the counting statistics for each energy spectra. In the present case, five angle bins are initially merged, leading to a single spectrum corresponding to an angular range of 0.4°. A further merging is carried out, aggregating ten such spectra, corresponding to a final angular window of 4°. The vertical lines drawn in the 2D spectrum shown in the inset of Fig. 1 represent the 4° window (between 118° and 122°), from which the energy

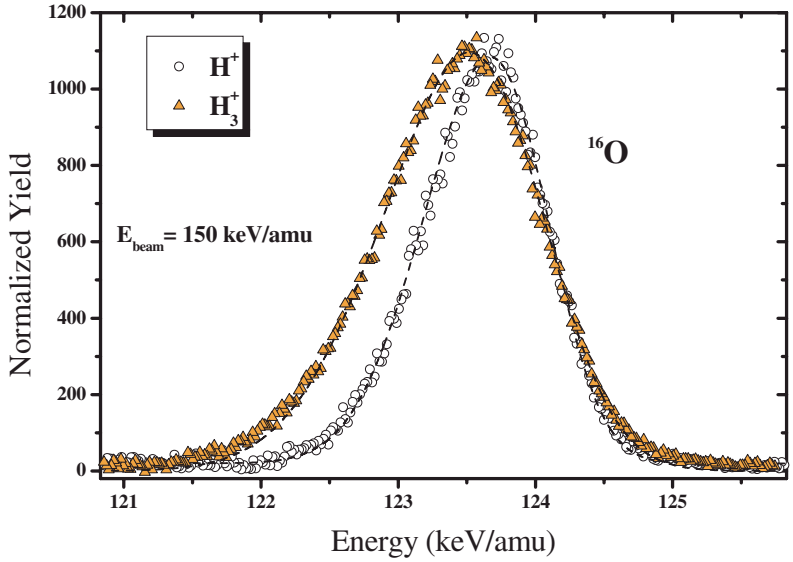

FIG. 2. (Color online) Typical 1D energy spectrum, similar to Fig. 1, but for 150 keV/amu H^+ and H_3^+ projectiles after background (due to channeling) subtraction. The best fit are indicated by dashed lines.

spectrum of Fig. 1 was derived. Every step of this procedure includes proper corrections, mainly due to different kinematical factors associated with each angle bin. Finally, three different angular windows of 4° each were selected, yielding three one-dimensional (1D) energy spectra for each experiment.

The 1D spectra were analyzed through the use of a simulation code developed for this purpose. Similar to other well-known programs,[26] this code takes into account all geometric factors and can handle several elements in bulk and layered targets. In short, this code calculates the probability of detecting an ion with a final energy E_f backscattered at a particular depth within the target assuming a Gaussian distribution for the energy loss. The mean energy loss and its variance along the incoming and outgoing straight-line trajectories are used as input parameters. Different options for background handling due to channeling alignment are available as well. The free parameters in the simulations are the target thickness, the energy loss, and the straggling. For the proton case, the values for the energy loss and straggling assumed in the simulations were allowed to vary in a restricted range around those values obtained from the SRIM 2003 code[7] and from the experimental published data,[27] respectively. For the cluster cases, the stopping parameters (energy loss and straggling) were adjusted in order to obtain the best fit of the respective energy spectrum. Once this step is accomplished, the stopping ratio between the cluster and the proton is then calculated.

As an example, Fig. 2 depicts a 1D spectra for 150 keV/amu H^+ and H_3^+ projectiles together with the best fits obtained through the procedure mentioned above. As can be observed from this figure, the backscattered particles in ^{16}O peak at about 123.5 keV/amu for both cases. However, the H_3^+ spectrum is much wider than that one for proton projectiles due to the larger energy loss of the H_3^+ projectiles at this energy. Also, the trailing and leading edges of the oxygen signal are broader for H_3^+ projectile as a consequence of the Coulomb explosion and Doppler effect due to molecular vibration before hitting the target.

The final results and respective uncertainties of the stopping ratios shown in Figs. 3–5 were evaluated in the following way: (i) between two and three independent measurements were carried out for each cluster energy; (ii) for each independent measurement, three 1D spectra were obtained; (iii) through the simulation code described above, each 1D spectrum yielded one stopping ratio, whose uncertainty was evaluated by changing the values of the stopping parameters and checking the goodness of the result; (iv) all stopping ratio values were averaged; and (v) finally, the uncertainties from steps (iii) and (iv) were convoluted, yielding uncertainties quoted in Figs. 3–5.

III. RESULTS AND DISCUSSION

The experimental results for the stopping ratios R_2 and R_3 are shown in Figs. 3 and 4. The general features are quite similar for both cases, featuring three distinct energy regions: (i) below 70 keV/amu, (ii) between 70 and 100 keV/amu, and (iii) above 100 keV/amu. In region (i), the stopping ratios R_2 and R_3 are compatible to each other and suggest a minimum value of about 0.82 and 0.87, respectively. In region (ii), a substantial increase in both stopping ratios is observed, while above 100 keV/amu, the ratios reach different values, namely, 1.23 and 1.52 for H_2^+ and H_3^+ cases, respectively.

We have carried out calculations of the stopping ratio R_n using the dielectric formalism.[11] These calculations make use of the so-called vicinage function in order to calculate the instantaneous stopping power of the constituents of the molecule as a function of the internuclear distance among them. The Lindhard dielectric function $\epsilon(\vec{k},\omega)$ (Ref. 28) and the Wigner-Seitz radius of $r_s=1.56$ (corresponding to the observed plasma frequency of SiO_2) were employed in such calculations. Binary (electron-hole) and plasmon excitations

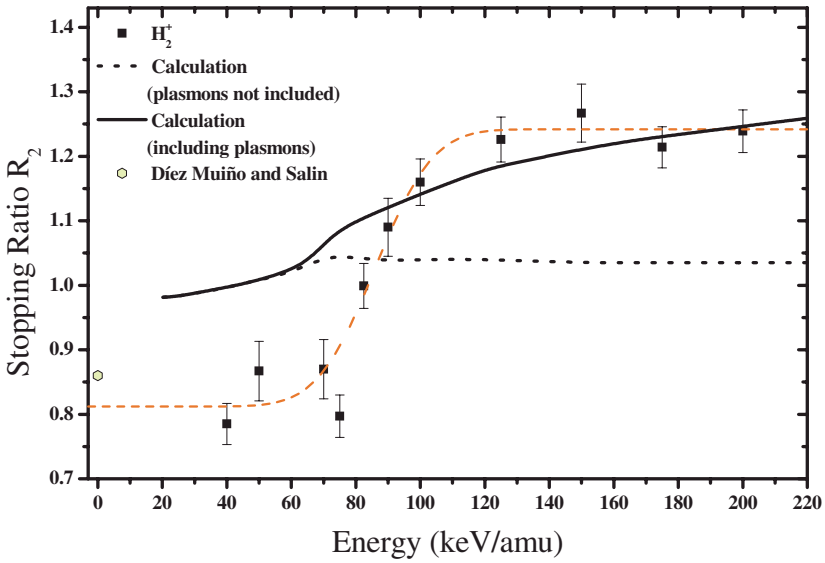

FIG. 3. (Color online) The experimental stopping ratio R_2 (full squares) as a function of the incident H_2^+ cluster energy. The thick lines represent the dielectric formalism calculations including plasmon excitations (full line) and without plasmon excitations (dotted lines) after averaging over charge-state fractions of H^+ and H^0 taken from CASP (Ref. 16). The open circle represents the result of the nonlinear calculation from Ref. 29. The dashed line is just to guide the eye through the experimental data of H_2^+ molecules.

were included in the calculations as well. Moreover, the fact that the Coulomb explosion is screened by the valence electrons of the solid was accounted for by the use of a screened Yukawa potential with $\alpha=(\pi/2)\omega_p/v$ as the screening constant, which depends on the ion velocity v and plasma frequency ω_p.

The fragmentation cross section for the present hydrogen clusters at the present energy range is large enough[14] to assure that all molecules are dissociated after entering the solid. Nevertheless, the charge state of each ionic fragment after dissociation will fluctuate toward a certain equilibrium value determined by capture and loss processes. Since the vicinage effect is very small in the case of fragments involving H^0, an average over the charge-state populations has to be considered for more accurate results. The charge-state fractions for the fragments after breakup were taken into account by considering the equilibrium values for hydrogen atoms as given by the CASP code[16] and uncorrelated charge-state fractions. For instance, in the case of H_2^+ projectiles, the fractions H^+H^+, H^+H^0, and H^0H^0 after breakup were considered to be the product of individual charge-state fractions. Nevertheless, tests using different charge-state distributions in the calculations did not show any significant energy shift or changes in the absolute values of R_n. It should be stressed that the conditions of the charge-state equilibrium can be affected by the presence of the close ions[11] in such a way that

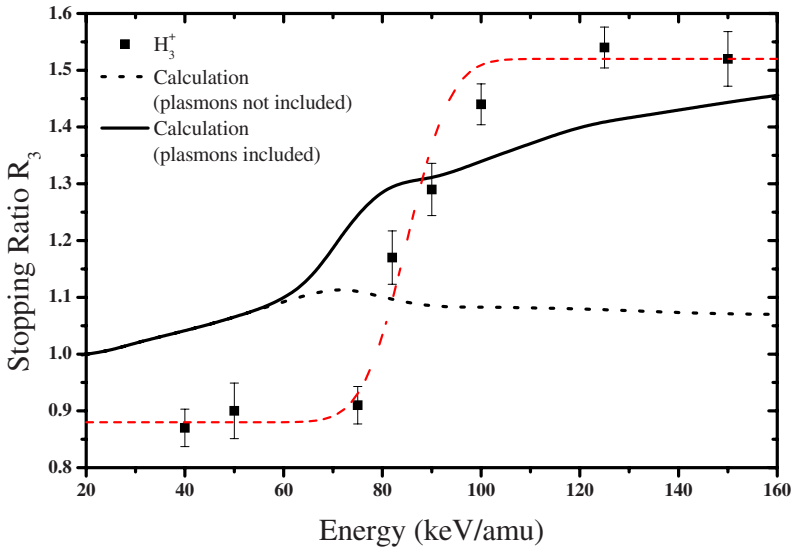

FIG. 4. (Color online) The same as Fig. 3, but for H_3^+ projectiles.

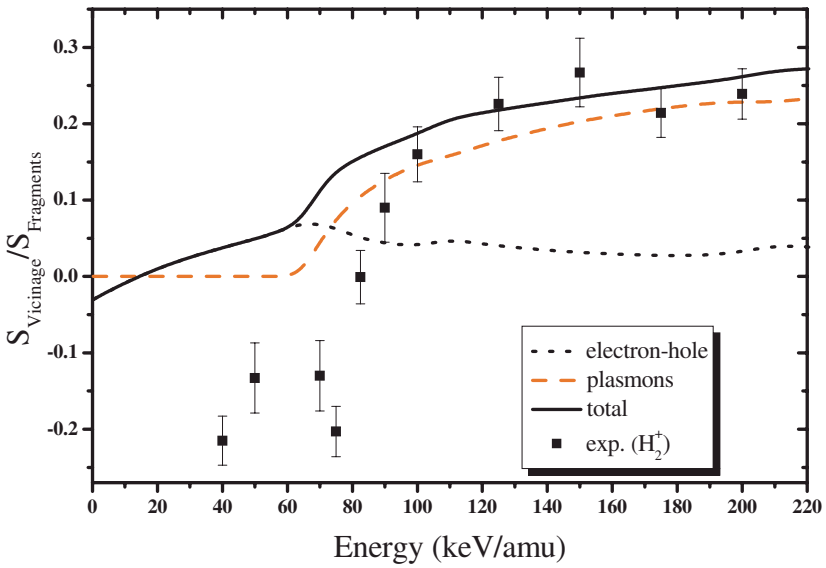

FIG. 5. (Color online) The vicinage effect divided by the stopping of uncorrelated fragments. The contribution of electron-hole and plasmon excitations are shown separately.

the initial charge states after the breakup (H^0) could prevail.

The results of such calculations are also displayed in Figs. 3 and 4 (full lines) for both R_2 and R_3, respectively. The dotted lines in these figures represent the same calculations, but without the contribution of plasmon excitation. Although there is a poor quantitative agreement between data and theory, the calculations show the thresholdlike behavior arising from the plasmon excitations. In addition, Fig. 5 shows the vicinage effect contribution to the stopping ratio R for fully ionized fragments (H^+) and the corresponding electron-hole and plasmon contributions. Here, the results were normalized to the energy loss of uncorrelated fragments. The lines represent the calculations for two protons traveling together, separated by 2.4 a.u. As can be observed from this figure, the threshold energy for plasmon excitation (the onset is about 60 keV/amu) is compatible with the experimental values obtained from Fig. 3 through the straightforward equation $S_v/S_f=1-R_2$. Furthermore, according to the linear response theory, the vicinage effect due to electron-hole excitations is very small and positive at low projectile energies, while our data show a negative interference. Finally, the same conclusions can be drawn for the H_3^+ data as well.

These results show the importance of plasmon excitations at high ion velocities. Below 100 keV/amu, the agreement is rather poor for both cases, where the linear theory overestimates the experimental results. However, it must be pointed out that, in this energy region where ion velocities are relatively low, higher-order effects come into play and the linear calculations based on the dielectric formalism break down. Moreover, the present calculations represent the state of art for the vicinage effect as a function of the projectile velocity. So far, there are no *ab initio* calculations for projectile energies between 50 and 200 keV/amu. Nevertheless, for very slow H_2^+ molecules, we can use the stopping values from the calculations developed by Díez Muiño and Salin[29] in order to assess the importance of such nonlinear effects. This model is based on the framework of the electron-hole pair excitations under adiabatic conditions as described in Ref. 30. Through the use of the Kohn-Sham theory, nonlinear effects in the response of the medium to the molecule and in the calculation of the scattering amplitudes are automatically taken into account as a function of internuclear axis direction. By averaging the parallel and perpendicular stopping ratios with respect to the center-of-mass velocity, we obtain the value shown in Fig. 3, which corresponds to ion speeds approaching zero. Such calculation yields a stopping ratio R_2 of 0.86, which is compatible with the asymptotic values of R_2, thus confirming the importance of nonlinear effects in the low velocity regime.

Figures 3–5 show that the onset of the sudden change in both stopping ratios happens at the same energy per nucleon, i.e., about 70 keV. This value corresponds to an ion threshold velocity of about $1.7v_0$, (v_0 is the Bohr velocity) and is quite large as compared to the one obtained from free-electron gas treatment (of about $1.3v_0$).[31] However, one must bear in mind that, in principle, charge-exchange processes as well as higher-order effects (in the electron-hole contribution) could affect the exact position of the threshold. Indeed, a rapid variation of the H^0 fraction could shift this position since the stopping ratio R_n for fragments involving H^0 is about 1. However, as discussed previously, tests using different charge-state distributions in the calculations did not show any significant energy shift.

Finally, it should be also stressed that plasmon excitations may also come from indirect processes such as secondary electrons produced in binary collisions with the target-valence electrons. Indeed, studies carried out with protons impinging at glancing incident angles on crystal Al[9] have shown that fast secondary electrons excited in the primary ion-target interaction appear to be an important channel for plasmon excitations even below the threshold ion energy. However, vicinage effects do not play any significant role for the production of delta electrons. Therefore, the stopping ratio R_n is only sensitive to direct processes of plasmon excitation.

IV. CONCLUSIONS

In summary, the energy region between 70 and 100 keV/amu is characterized by an increase of about 50% and 75% of the stopping ratio values for both H_2^+ and H_3^+ clusters, respectively. A comparison between the data and calculations based on the dielectric formalism indicates that, indeed, this increase may be the signature of a strong plasmon excitation contribution to the stopping power. The increase in the stopping ratio values predicted by the calculations amounts to around 17% and 32% for H_2^+ and H_3^+ clusters, respectively. Although these results do not match the experimental values, both theory and experiment point to a larger contribution of the plasmon excitations to the stopping ratio in the case of the H_3^+ ionic cluster. In general, the dielectric formalism fails to explain the low energy region and the sudden change in the stopping ratio, while at higher energies, the model appears to be consistent with data, which further corroborates the important role played by the plasmon excitations. The overall results obtained for energy regions (i) and (ii) suggest that different mechanisms are important for the description of vicinage effect. In region (i), one could argue that nonlinear screening effects due to the scattering of the electrons in the first proton of the cluster could lead to an enhancement of the electron density for the trailing protons which, in turn, would decrease the stopping for such protons. For region (ii), one could speculate on the role of charge-exchange processes near the plasmon threshold energy. One possible explanation of the sudden change in the stopping ratio values may reside in the stronger nonlinear effects not present in the dielectric model. Therefore, it would be important to extend the nonlinear calculations (so far restricted to low energies) to a wide range of energies in order to search for a possible explanation of this unexpected behavior.

ACKNOWLEDGMENTS

This research was supported by Conselho Nacional de Desenvolvimento Científico e Tecnológico (CNPq) and Fundação de Amparo à Pesquisa do Estado do Rio Grande do Sul (FAPERGS).

[1] J. M. Pitarke, V. M. Silkin, E. V. Chulkov, and P. M. Echenique, Rep. Prog. Phys. **70**, 1 (2006).
[2] K. Sasaki, S. Tsukimoto, M. Konno, T. Kamino, and H. Saka, J. Microsc. **203**, 12 (2001).
[3] E. B. Priestley, B. Abeles, and R. W. Cohen, Phys. Rev. B **12**, 2121 (1975).
[4] C. H. Chen, J. Silcox, and R. Vincent, Phys. Rev. B **12**, 64 (1975).
[5] J. H. Kim, J. J. Sanchez, T. A. DeMassa, M. T. Quddus, D. Smith, F. Shaapur, K. Weiss, and C. H. Liu, J. Appl. Phys. **84**, 1430 (1998).
[6] R. A. Baragiola, C. A. Dukes, and P. Riccardi, Nucl. Instrum. Methods Phys. Res. B **182**, 73 (2001).
[7] J. F. Ziegler, J. P. Biersack, and U. Littmark, *The Stopping and Range of Ions in Solids* (Pergamon, New York, 1985). The SRIM code is available at www.srim.org.
[8] S. M. Ritzau, R. A. Baragiola, and R. C. Monreal, Phys. Rev. B **59**, 15506 (1999).
[9] E. A. Sanchez, J. E. Gayone, M. L. Martiarena, O. Grizzi, and R. A. Baragiola, Phys. Rev. B **61**, 14209 (2000).
[10] N. J. Zheng and C. Rau, J. Vac. Sci. Technol. A **11**, 2095 (1993).
[11] N. R. Arista, Nucl. Instrum. Methods Phys. Res. B **164-165**, 108 (2000).
[12] D. S. Gemmell, J. Remillieux, J. C. Poizat, M. J. Gaillard, R. E. Holland, and Z. Vager, Phys. Rev. Lett. **34**, 1420 (1975).
[13] W. Brandt, A. Ratkowski, and R. H. Ritchie, Phys. Rev. Lett. **33**, 1325 (1974).
[14] N. V. de Castro Faria, I. Borges, Jr., L. F. S. Coelho, and G. Jalbert, Phys. Rev. A **51**, 3831 (1995).
[15] I. D. Williams, J. Geddes, and H. B. Gilbody, J. Phys. B **17**, 811 (1984).
[16] P. L. Grande and G. Schiwietz, Phys. Rev. A **58**, 3796 (1998). The CASP code is available at www.hmi.de/people/schiwietz/casp.html.
[17] J. M. Caywood, T. A. Tombrello, and T. A. Weaver, Phys. Lett. **37A**, 350 (1971).
[18] J. C. Poizat and J. Remillieux, J. Phys. B **5**, L94 (1972).
[19] T. A. Tombrello and J. M. Caywood, Phys. Rev. B **8**, 3065 (1973).
[20] V. A. Khodyrev, V. S. Kulikauskas, and C. Yang, Nucl. Instrum. Methods Phys. Res. B **195**, 259 (2002).
[21] R. C. Fadanelli, P. L. Grande, M. Behar, J. F. Dias, G. Schiwietz, and C. D. Denton, Phys. Rev. B **69**, 212104 (2004).
[22] R. M. Tromp, H. H. Kersten, E. Granneman, R. Koudijs, and W. J. Kilsdonk, Nucl. Instrum. Methods Phys. Res. B **4**, 155 (1984).
[23] R. P. Pezzi, C. Krug, E. B. O. da Rosa, J. Morais, L. Miotti, and I. J. R. Baumvol, Nucl. Instrum. Methods Phys. Res. B **190**, 510 (2002).
[24] R. M. Tromp, M. Copel, M. C. Reuter, M. H. Von Hoegen, J. Speidell, and R. Koudijs, Rev. Sci. Instrum. **62**, 2679 (1991).
[25] R. G. Smeenk, R. M. Tromp, H. H. Kersten, A. J. H. Boerboom, and F. W. Saris, Nucl. Instrum. Methods Phys. Res. **195**, 581 (1982).
[26] E. Rauhala, N. P. Barradas, S. Fazinic, M. Mayer, E. Szilágyi, and M. Thompson, Nucl. Instrum. Methods Phys. Res. B **244**, 436 (2006).
[27] J. H. R. dos Santos, P. L. Grande, M. Behar, J. F. Dias, N. R. Arista, J. C. Eckardt, and G. H. Lantschner, Phys. Rev. A **68**, 042903 (2003).
[28] J. Lindhard, Mat. Fys. Medd. K. Dan. Vidensk. Selsk. **28**, 8 (1954).
[29] R. Díez Muiño and A. Salin, Phys. Rev. B **62**, 5207 (2000).
[30] M. Lindenblatt, E. Pehlke, A. Duvenbeck, B. Rethfeld, and A. Wucher, Nucl. Instrum. Methods Phys. Res. B **246**, 333 (2006).
[31] D. Pines, *Elementary Excitations in Solids* (Benjamin, New York, 1964).